SCIENCE CHINA
Technological Sciences

Progress of Projects Supported by NSFC

May 2012 Vol.55 No.5: 1327–1334
doi: 10.1007/s11431-012-4764-2

Effect of solidification rate on competitive grain growth in directional solidification of a nickel-base superalloy

ZHOU YiZhou & SUN XiaoFeng*

Institute of Metal Research, Chinese Academy of Sciences, Shenyang 110016, China

Received December 7, 2011; accepted January 17, 2012; published online February 23, 2012

The mechanism of grain structure evolution during directional solidification is a fundamental subject in material science. Within the published research there exist conflicting views on the mechanism of grain overgrowth. To study the effect of solidification rate on grain structure evolution, bi-crystals samples were produced in a nickel-base superalloy at different solidification rates. It was found that at the convergent grain boundaries those grains better aligned with respect to the heat flux more readily overgrew neighbouring grains with misaligned orientations and the effect became more pronounced as solidification rate was increased. However, at diverging grain boundaries the rate of overgrowth was invariant to the solidification rate. These experimental results were compared with models in the literature. Thus, a better insight into competitive grain growth in directional solidification processes was obtained.

competitive grain growth, structure evolution, directional solidification, nickel alloys

Citation: Zhou Y Z, Sun X F. Effect of solidification rate on competitive grain growth in directional solidification of a nickel-base superalloy. Sci China Tech Sci, 2012, 55: 1327–1334, doi: 10.1007/s11431-012-4764-2

1 Introduction

It has been widely reported that a preferred crystallographic orientation is produced in as-cast components after directional solidification (DS) and such a preferred orientation is the fast-growing dendritic orientation [1–14]. For the alloys with face centered cubic structure, ⟨001⟩ is the fast-growing orientation. Thus, the DS structure in nickel-base superalloys is presented in the form of ⟨001⟩ texture [15–17]. Study of the development of a solidification texture originated from the work of Walton and Chalmers published in 1959 [1]. They used bi-crystal samples of lead and silver to study the grain structure evolution in DS process and suggested that grains oriented favourably and unfavourably with respect to the thermal gradient grow at different undercoolings. To maintain their relative position with respect to an advancing liquidus, misaligned grains grow at greater undercoolings, i.e., the misaligned grains lag behind the better aligned neighbours. The difference on undercooling creates the condition enabling grain overgrowth and then leads to the formation of solidification texture. The idea of different undercoolings controlling texture formation during columnar grain growth has found widespread acceptance. However, within the literature there are different explanations of the overgrowth process.

Figure 1(a) shows the first explanation of overgrowth process [18]. The dendrites in the better aligned grain A lead the dendrites in the misaligned grain B; under this condition a secondary dendrite from the leading dendrite develops and blocks the growth of misaligned dendrites at the grain boundary (GB) of the converging grains. As a new tertiary/primary dendrite is developed from the elongated secondary dendrite at the GB due to branching, grain A extends laterally to overgrow grain B.

*Corresponding author (email: xfsun@imr.ac.cn)

The second explanation of overgrowth process is illustrated in Figure 1(b) [19, 20]. For the two grains on the left, the primary dendrite trunks are converging and the growth of the dendrites in the misaligned grain B is stopped by the better aligned grain A_1 at the GB. Since grain A_1 does not develop new dendrites at the GB and the dendrites in grain B cannot overgrow the dendrites in grain A_1, the GB lies in parallel to the dendrite trunks in grain A_1. For the two grains on the right, the dendrite trunks are diverging. The open GB region allows secondary and tertiary dendrite arms to develop from both grains and dendrite development from the better aligned grain A_2 leads to overgrowth of grain B. Since grain B cannot expand to the left, it is gradually overgrown from the right and disappears over some distance.

In our work [21], the structure evolution of bi-crystal (BC) samples during DS processing was explored in an attempt to understand the mechanism of competitive grain growth. The experimental results are summarized in Figure 1(c). In the case of converging dendrites our experiments had the following results. Firstly, new dendrites hardly developed from either grain at the GB. This result is not in accordance to Figure 1(a), but to Figure 1(b) (the two grains on the left). Secondly, the primary dendrites at the GB were growing behind their immediate neighbours in the form of a groove. Thus, the misaligned dendrites were able to overgrow the better aligned dendrites. This result differs from Figures 1(a) and (b). Thirdly, the misaligned grain was able to overgrow the better aligned grain by blocking the dendrites of the better aligned grain at the GB. This result disagrees with Figures 1(a) and (b). In the case of diverging dendrites, our experimental results were in accordance with Figure 1(b) (the two grains on the right).

Since the growth conditions used by different authors were different, we wondered if the conflicts summarised in Figure 1 are due to the varying casting parameters, such as different solidification rate (i.e. different withdrawal speed). To understand the effect of solidification rate on competitive grain growth, different withdrawal speeds were used to produce BC samples in the present work. By comparing the structure evolutions in BC samples with different withdrawal speeds, a better insight on competitive grain growth in DS process was obtained.

2 Experiments

2.1 Materials and arrangement of seeds

The compositions of the materials used in the present work are listed in Table 1.

SC seeds from superalloy PWA1483 were used to control the orientations in the BC casting process. Since PWA1483 is the SC equivalent of IN792, having almost the same composition except the minor elements B and Zr, PWA1483 seeds do not influence the nominal composition of IN792 after casting [22]. Each seed was cut into two halves along the sample axis. Subsequently, the seeds were arranged in such a way that the samples with converging or diverging primary dendrites were produced. To simplify microstructural analysis, both ⟨001⟩ directions in the BC samples were kept on the same plane. In the present work, grain A was always better aligned to the thermal gradient

Table 1 Nominal compositions of alloys as used in the experiments (in weight percent)

Alloy	IN792	PWA1483
Cr	12.5	12.2
Co	8.8	9.0
Mo	1.8	1.9
W	4.0	3.8
Al	3.4	3.6
Ti	3.9	4.2
Ta	3.9	5.0
B	0.014	0
Zr	0.017	0
C	0.08	0.07
Ni	Bal.	Bal.

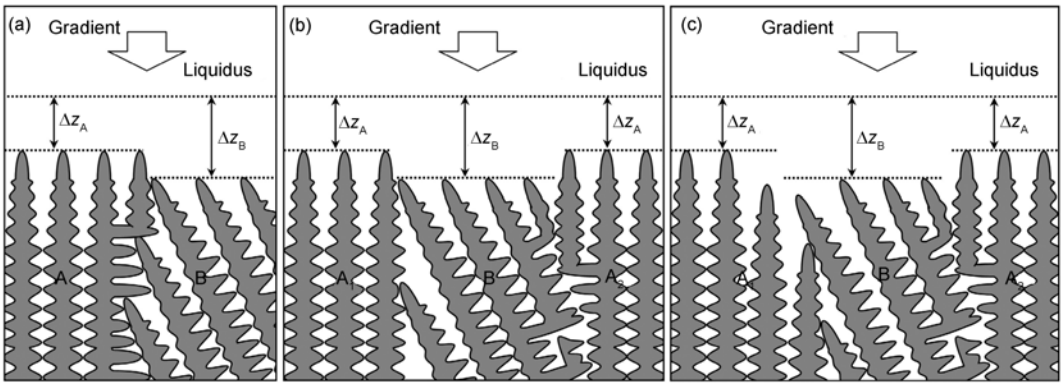

Figure 1 Schematic diagrams showing the models for competitive grain growth in DS process in literature. (a) from ref. [18]; (b) from refs. [19, 20]; (c) from ref. [21].

Table 2 Structural characteristics and casting conditions of the samples

Exp.	Nature of sample	Seed disposition	θ_A (°)	θ_B (°)	Withdrawal speed (mm/min)
Exp. 1(a)	HRS BC	convergence	7±1	−19±1	1
Exp. 1(b)	HRS BC	convergence	7±1	−19±1	6
Exp. 2(a)	HRS BC	convergence	0±1	−19±1	1
Exp. 2(b)	HRS BC	convergence	0±1	−19±1	6
Exp. 3(a)	LMC BC	convergence	0±1	−10±1	1
Exp. 3(b)	LMC BC	convergence	0±1	−10±1	6
Exp. 4 (a)	HRS BC	divergence	6±1	22±1	1
Exp. 4(b)	HRS BC	divergence	6±1	22±1	6
Exp. 5(a)	HRS BC	divergence	0±1	21±1	1
Exp. 5(b)	HRS BC	divergence	0±1	21±1	6
Exp. 6(a)	LMC BC	divergence	0±1	9±1	1
Exp. 6(b)	LMC BC	divergence	0±1	9±1	6

than grain B. θ_A and θ_B were used to describe the misorientations of ⟨001⟩ direction from the sample axis in seeds A and B, respectively. θ_A and θ_B were defined to be plus when they were inclined from the better aligned grain A to the misaligned grain B because such inclination of ⟨001⟩ direction was helpful for that grain A overgrew grain B. In contrast, θ_A and θ_B were defined to be minus when they were inclined from the misaligned grain B to the better aligned A. The details of θ_A and θ_B in the experiments are listed in Table 2. It is clear from Table 2 that $|\theta_A| < |\theta_B|$.

2.2 Casting experiments

A Bridgman high rate solidification (HRS) furnace was used to conduct BC casting experiments under a vacuum environment. Samples were produced in a mould comprising a pure alumina tube mounted vertically upon a water-cooled copper chill plate. The cast samples were cylindrical, with diameter of 10 mm and length of 150 mm. BC seeds of length of 20–25 mm were inserted into the bottom of the mould. After preheating to 1500°C, to partially re-melt the seeds along their length, an IN792 charge was melted and superheated to 1550°C and held at temperature for 5 min. The temperature was reduced to the casting temperature (1500°C) and the melt was poured into the preheated mould. After 2-minutes of holding, to allow the system to attain a thermal equilibrium, the assembly was withdrawn at a constant rate of 1 mm/min or 6 mm/min.

To study the microstructure in the mushy zone, quenched BC experiments were performed by using a liquid metal cooling (LMC) furnace. The alumina mould with BC seeds in the bottom was mounted on a steel chill plate. BC samples with diameter of 12 mm were directionally solidified into a tin bath for a height of 50 mm at withdrawal speeds of 1 mm/min and 6 mm/min then rapidly quenched into the bath at a withdrawal speed of 120 mm/min, thereby freezing the microstructure of the mushy zone.

2.3 Sample examination

Macroetching was employed to determine the positions of the melt-back interface and grain boundary. The GB inclination angle (θ_{GB}) to the withdrawal axis was determined by $\tan\theta_{GB} = R/L$, where R is the travelling distance of the GB from the initial position (determined on a cross section) and L is the corresponding distance from the melt-back interface to the determined cross section. To reduce the experimental error, L was as long as possible ($\geqslant$ 50 mm). In accordance with the convention defined previously, θ_{GB} was defined to be plus when the GB plane was inclined in such a way that the better aligned grain A overgrew the misaligned grain B and θ_{GB} was defined to be minus when the GB plane was inclined in such a way that the misaligned grain B overgrew the better aligned grain A. Subsequently, BC samples were cut and polished to show the microstructures. θ_A and θ_B were examined on longitudinal sections. The primary dendrite arm spacing (λ_1) was determined on horizontal sections.

3 Results

3.1 BC samples with converging dendrites

λ_1 in BC samples are summarized in Table 3. As solidification rate increased, λ_1 was reduced in the casting experiments. Values of λ_1 measured in HRS and LMC BC samples were almost identical at the same solidification rate.

Figure 2 shows the optical metallographic microstructure of Experiment 1. The orientations were the same in Experiments 1(a) and (b), while the withdrawal speeds were different. At the low withdrawal speed (1 mm/min), the following results can be concluded from experimental observations (Figure 2(a)). Firstly, new dendrites were hard to develop from both grains at the GB. Secondly, not only

Table 3 Primary dendrite arm spacing (λ_1) in BC samples

Withdrawal speed	λ_1 (μm)				
	HRS			LMC	
	0° dendrites	6° dendrites	22° dendrites	0° dendrites	10° dendrites
1 mm/min	285	282	282	268	274
6 mm/min	184	175	183	175	176

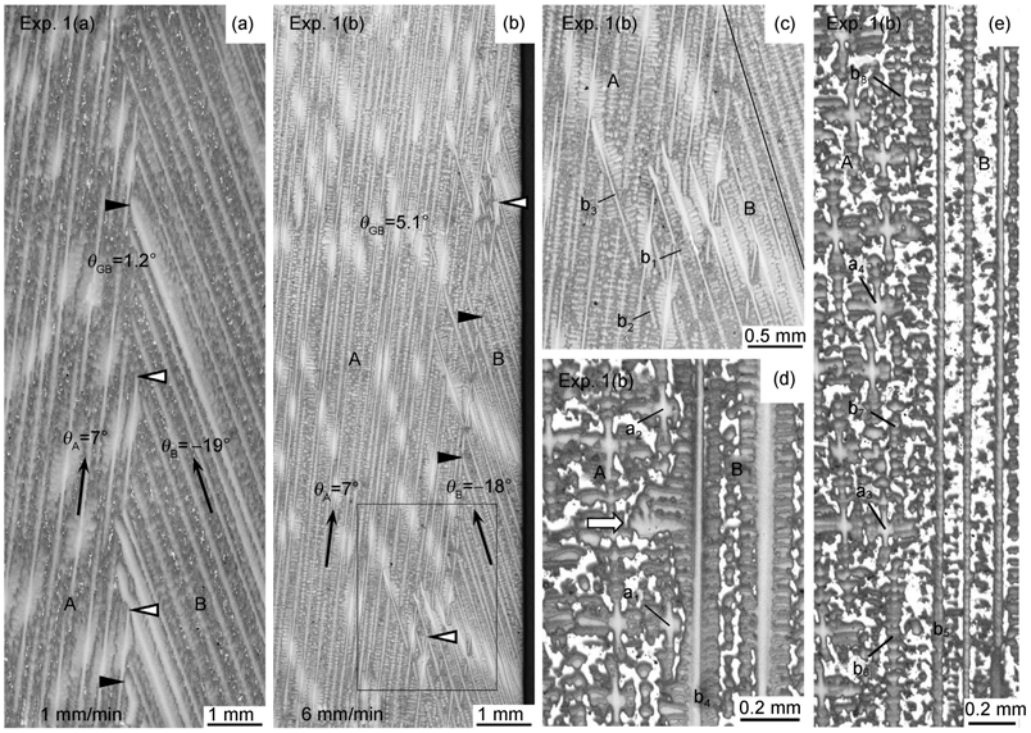

Figure 2 Optical micrographs showing the microstructures in Experiment 1. (a) 1 mm/min withdrawal speed; (b) 6 mm/min withdrawal speed; (c) the detailed microstructure in the black frame in (b), (d) and (e) microstructures on the section cut along the [001] direction of grain B in the sample solidified at 6 mm/min.

were the better aligned dendrites able to block the misaligned dendrites, but also the misaligned dendrites were able to block the better aligned dendrites. Thirdly, the GB was nearly parallel to the sample axis and grain B did not disappear at the sample top (150 mm from the melt-back interface). The GB inclination angle θ_{GB} was 1.2°.

A general view of the GB structure at a high withdrawal speed (6 mm/min) is shown in Figure 2(b) and the detailed GB structure marked by the dark frame in Figure 2(b) is presented in Figure 2(c). The followings were observed from Figures 2(b) and (c). Firstly, the grain boundary was less clearly defined, with primary stems apparently impeded and subsequently re-established. This gave rise to the interwoven or overlapping structure appeared in the first instance. Secondly, not only were the better aligned dendrites able to block the misaligned dendrites, but also the misaligned dendrites were able to block the better aligned dendrites. This is the same as the result at the low solidification rate. Thirdly, the GB was inclined from grain A to grain B and the GB inclination angle θ_{GB} was 5.1°. This result indicates that at a higher solidification rate grain overgrowth occurred at a greater rate.

To understand the mechanism of evolution of the interwoven or overlapping structure in Experiment 1(b), the microstructure on the section cut along the [001] direction in grain B (an example of which was marked by the straight line in Figure 2(c)) was studied and the observations are shown in Figures 2(d) and (e). The dendrites in grain A appeared as crosses and the dendrites in grain B appeared as straight stems. In Figure 2(d), dendrites a_1 and a_2 were on the longitudinal plane 1 and dendrite b_4 was on another longitudinal plane 2. The secondary arms of dendrite b_4 extended from plane 2 into plane 1 and impinged into the gap of dendrites a_1 and a_2 (highlighted by an arrow). Thus, on the longitudinal plane 1 (i.e. the plane of Figures 2(b) and (c)) a short dendrite of grain B can be observed between two dendrites of grain A (example of which was marked by dendrite b_1 in Figure 2(c)). In Figure 2(e), the growth of dendrite b_6 on longitudinal plane 1 was stopped by dendrite a_3. However, above dendrite a_3, a new dendrite b_7 (on longitudinal

plane 1) was developed from dendrite b_5 (on another longitudinal plane 2) due to branching. The growth of dendrite b_7 was stopped by dendrite a_4 and a new dendrite b_8 was developed from dendrite b_5 in the subsequent solidification process. Obviously, the dendrites b_2 and b_3 in Figure 2(c) were formed by this mechanism.

The experimental results in Experiments 2 and 3 are similar to those in Experiment 1. At the low withdrawal speed (1 mm/min), side arm growth was suppressed and new dendrites were hard to develop at the GB and the misaligned dendrites could block the better aligned dendrites; the GB was inclined in such a way that grain B overgrew grain A in Experiments 2(a) and 3(a). At the high withdrawal speed (6 mm/min), new dendrites could develop at the GB and branching to form new primary stems from grain A reduced the rate of overgrowth of grain A by grain B; the GB was nearly parallel to the sample axis and both grains survived in the solidified length in Experiments 2(b) and 3(b), i.e. grain A was more competitive and grain B was less competitive at a higher solidification rate. The microstructure of the mushy zone in Experimemnt 3 is presented in Figure 3. Dendrite development was not observed in the GB region at the low solidification rate. However, new dendrites could develop at the high solidification rate. Likewise, the positions where new dendrites began appearing were behind the "blocked" dendrite tips in the other grain.

The dependence of GB inclination angle θ_{GB} on withdrawal speed in the case of converging dendrites is summarised in Figure 4. θ_{GB} is positive in Experiment 1, showing that grain A overgrew or tended to overgrow grain B. θ_{GB} was negative in Experiments 2 and 3, showing that grain B overgrew or tended to overgrow grain A. As the solidification rate increased, θ_{GB} increased, i.e., the well aligned grain (A) became more competitive. In Experiments 1(a), 2(b) and 3(b), θ_{GB} was close to 0, showing that the GB was nearly parallel to the sample axis and thus both grains survived in the whole casting process. As shown in Table 2, Experiments 1 and 2 were cast by HRS technique and Experiment 3 was cast by LMC technique. Obviously, the effect of solidification rate on microstructure evolution was the same under different casting techniques.

3.2 BC samples with diverging dendrites

Figure 5 shows the optical metallographic microstructure of Experiment 4. The GB structures at different solidification rates are similar to each other. New dendrites developed from grains A and B at the GB and the gap of the diverging

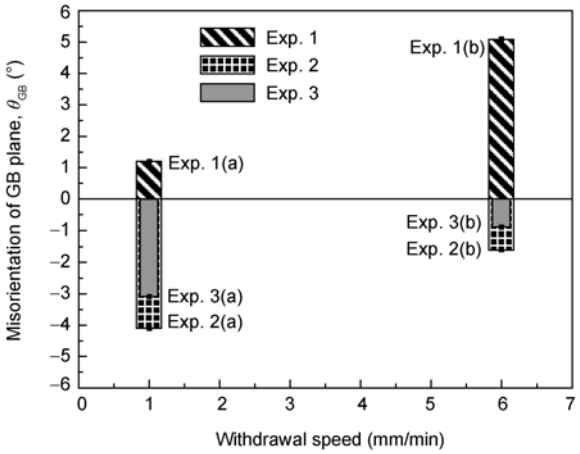

Figure 4 Dependence of θ_{GB} on withdrawal speed in the case of converging dendrites.

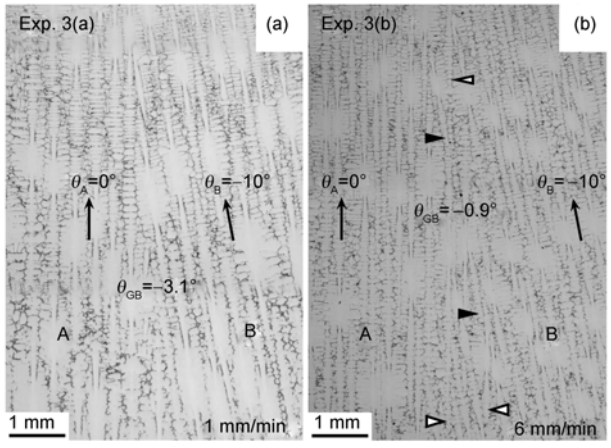

Figure 3 Optical micrographs showing the microstructures of mushy zones in Experiement 3. (a) 1 mm/min withdrawal speed; (b) 6 mm/min withdrawal speed.

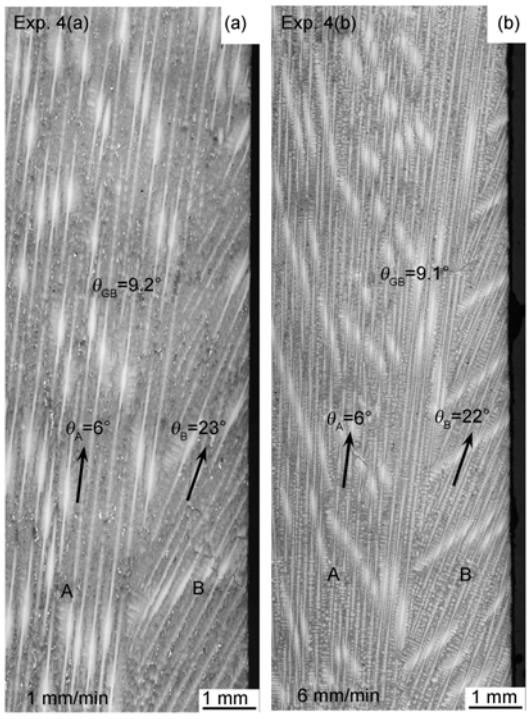

Figure 5 Optical micrographs showing the microstructures in Experiment 4. (a) 1 mm/min withdrawal speed; (b) 6 mm/min withdrawal speed.

grains was filled by these new dendrites. The dendrites of grain A and grain B did not overlap into grains B and A, respectively. The GB was inclined in such a way that grain A overgrew grain B. The rates of grain overgrowth at different solidification rates were the same and the GB inclination angle θ_{GB} was 9.2°, i.e., within the range of growth rates studied θ_{GB} was invariant with respect to withdrawal velocity.

The experimental results in Experiments 5 and 6 are similar to those in Experiemnt 4, i.e., new dendrites developed from grains A and B at the GB; the dendrites of one grain could not impinge in the other grain and θ_{GB} was the same at different solidification rates.

The dependence of the GB inclination angle θ_{GB} on withdrawal speed in the case of diverging dendrites is summarised in Figure 6. θ_{GB} is always positive, showing that grain A always overgrew or tended to overgrow grain B in the case of diverging dendrites. As the orientations in BC samples were the same, the solidification rate did not affect θ_{GB}. This mechanism is the same using different casting techniques.

4 Discussion

4.1 Overgrowth in the case of converging dendrites

If dendrites at the converging GB can develop new dendrites on the same longitudinal plane towards the GB by means of branching effect, the positions where the new dendrites begin appearing should be ahead of the blocked dendrite tips (in the other grain) as shown in Figure 1(a). However, in Experiments 1(b), 2(b) and 3(b) the positions where the new dendrites began appearing were behind the blocked dendrite tips and led to a structure with 'interwoven' appearance. This result indicates that the new dendrites at the converging GB did not develop from the dendrites on the same longitudinal plane. As confirmed in Figures 2(d) and (e), the new dendrites developed from the dendrites on another longitudinal plane. Obviously, the development of dendrites did not follow the mechanism as shown in Figure 1(a).

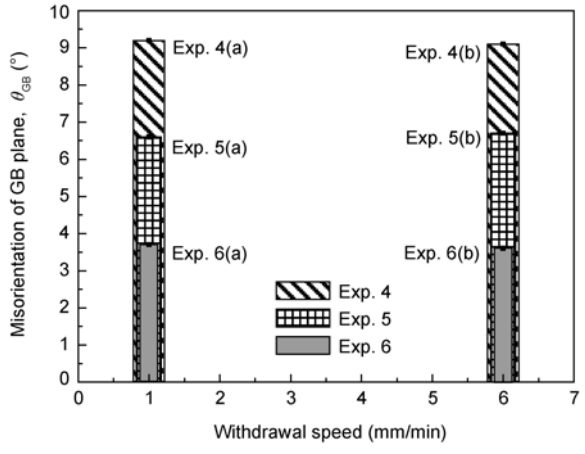

Figure 6 Dependence of θ_{GB} on withdrawal speed in the case of diverging dendrites.

The present work demonstrated that the branching effect from different longitudinal planes is dominated by the withdrawal speed V. Generally, it is accepted that the primary dendrite arm spacing λ_1 is proportional to $V^{-0.25}$ and the solute field range δ of a dendrite is proportional to V^{-1} [23]. Thus, λ_1/δ is proportional to $V^{0.75}$ and a greater V leads to a higher ratio of λ_1/δ. This means that at a higher withdrawal speed there is a wider gap between two neighbouring dendrites, enabling the impingement of dendrite arms from another grain. On the aspect of dendrite morphology, the secondary dendrite arms are well developed (fine and long) at the high withdrawal speed, whilst they are undeveloped (coarse and short) at the low solidification rate. Consequently, the branching effect on different longitudinal planes was observed more frequently at the high solidification rate.

The interwoven structure of dendrites has been observed in the previous work [24] and the structure evolution has been illustrated schematically there. However, the experimental result in [24] was not as rich as that presented here. To well understand the mechanism of interwoven structure development, the schematic illustration in ref. [24] is recalled to compare with the GB structure evolution in Experiment 1(b); see Figure 7. The white and grey dendrites lie on adjacent planes 1 and 2, respectively. Plane 2 is behind plane 1, separated by a distance of λ_1. The grey dendrites on plane 2 extend into plane 1 and developed new dendrites on plane 1, as highlighted by arrows a_1 and a_2 in Figure 7(b). Likewise, the white dendrites on the plane 1 extend their branches to plane 2 and developed new dendrites on plane 2 as pointed out by arrows b_1 and b_2 in Figure 7(c).

Since grain A is more favourably oriented, a great number of new dendrites developed from grain A are able to block the dendrites in grain B at the GB. In contrast, few dendrites developed from grain B are able to block the dendrites in grain A at the GB. Thus, dendrite development from grain A causes a GB inclination θ_{dev} from grain A to grain B. Following our convention, θ_{dev} is positive. However, in the case of converging grains the misaligned dendrites are able to overgrow the better aligned dendrites at different solidification rates. Blocking of the better aligned dendrites by the misaligned dendrites at the GB leads to inclination of the GB by an amount θ_{blo} from grain B to grain A. Following our convention, θ_{blo} is negative. Consequently, θ_{GB} can be written as $\theta_{GB} = \theta_A + \theta_{dev} + \theta_{blo}$. At the low solidification rate, since θ_{dev} is very small or equal to 0 (i.e., dendrites are hard to develop at the GB), the minus θ_{blo} leads to $\theta_{GB} < \theta_A$. In Experiment 1(a), the result of $\theta_{GB} < \theta_A$ is that the GB was nearly parallel to the sample axis. In

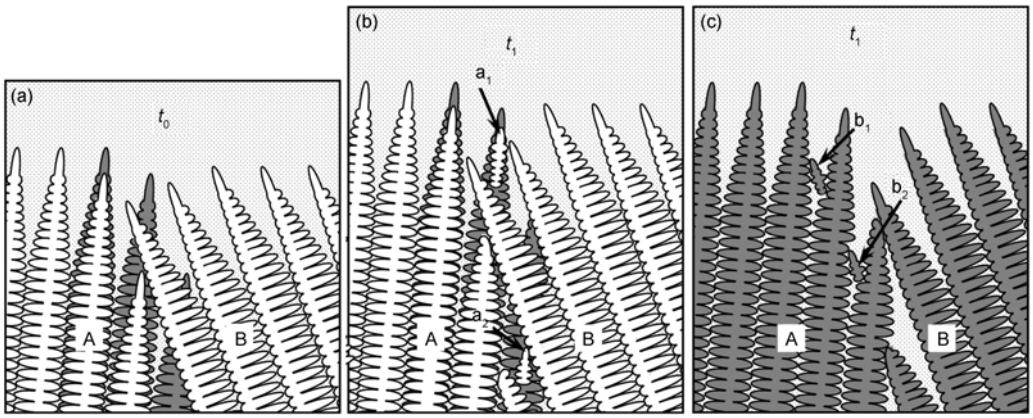

Figure 7 Schematic diagram showing the structure evolution in Experiment 1, from [24]. (a) Grain boundary structure containing two longitudinal planes at time t_0; (b) grain boundary structure containing two longitudinal planes at time t_1; (c) grain boundary structure containing one longitudinal plane at time t_1.

Experiemnts 2(a) and 3(a), the result of $\theta_{GB} < \theta_A$ is that the GB was inclined in such a way that grain B overgrew grain A. At the high solidification rate, the addition of plus θ_{dev} and minus θ_{blo} may be very small or equal to 0. Thus, θ_{GB} may be very close or equal to θ_A. In Experiment 1(b), the result of θ_{GB} close to θ_A is that grain B disappeared over some distance. In Experimemnts 2(b) and 3(b), the result of θ_{GB} close to θ_A is that the GB was nearly parallel to the sample axis. However, $\theta_{GB} \approx \theta_A$ (or $\theta_{GB}=\theta_A$) at the high solidification rate is not due to the mechanism as shown in Figure 1(b).

With detailed review of Figure 14 in the work of Walton and Chalmers [1], it can be found that the structure evolution of the BC sample with converging grains was indeed like that illustrated in Figure 3(b), i.e., the better aligned dendrites were impeded and subsequently re-established at the GB. Thus, there was no marked GB inclination from the better aligned dendrite trunks and the rate of overgrowth was thereby negligible.

As reported in the previous work [21] and summarized in Figure 1(c), the GB groove of converging grains is the reason why the misaligned dendrites are able to overgrow the better aligned dendrites. Interaction between the overlapping solute fields is the most probable factor for the presence of the GB groove [21]. Since the solute field range δ of a dendrite reduces with the increasing withdrawal speed ($\delta \propto V^{-1}$), the GB groove should be smaller at the higher withdrawal speed, thereby reducing the likelihood of overgrowth of better aligned dendrites by the misaligned dendrites. This effect may therefore explain why the better aligned grains more readily overgrew neighbouring grains with misaligned orientations as solidification rate is increased.

4.2 Overgrowth in the case of diverging dendrites

At different solidification rates, the results in the samples with diverging dendrites are in accordance with Figures 1(b) and (c). Unlike the case of converging dendrites, the dendrites of grains A and B do not impinge upon each other at any solidification rate. In the schematic representation of an expanding GB region (Figure 8), the bright dendrite a_1 on plane 1 and the grey dendrite a_2 on plane 2 have the same probability to develop a new dendrite a at the GB on plane 1 (the distances from dendrite a to a_1 and a_2 are nearly the same); see Figure 8. Likewise, the bright dendrite b_1 on plane 1 and the grey dendrite b_2 on plane 2 have the same probability to develop a new dendrite b at the GB on plane 2. The characteristics of secondary arms do not affect the branching effect thereby in the case of diverging dendrites θ_{GB} are the same at different solidification rates.

Since there is no dendrite blocking ($\theta_{Blo} = 0$) at the GB of diverging grains, θ_{GB} can be written as $\theta_{GB} = \theta_A + \theta_{Dev}$. The present work shows that θ_{Dev} is independent of the solidification rate in the case of diverging dendrites and is instead a function of θ_A and θ_B only.

5 Conclusions

It has been found that the effect of solidification rate on grain structure evolution during directional solidification is different in the BC samples with converging and diverging grains.

I. In the case of converging grains, grain overgrowth behaviours and rate change as the solidification rate varies. At higher solidification rates grains better aligned to the heat flux become more competitive and misaligned grains less competitive in the growth process. This is attributed to varying branching effect at different longitudinal planes. Since the branching effect at different longitudinal planes is enhanced and new dendrites are easier to develop at the converging GB, the better aligned grains have more chances to survive at the higher solidification rate.

II. In the case of diverging grains, the solidification rate

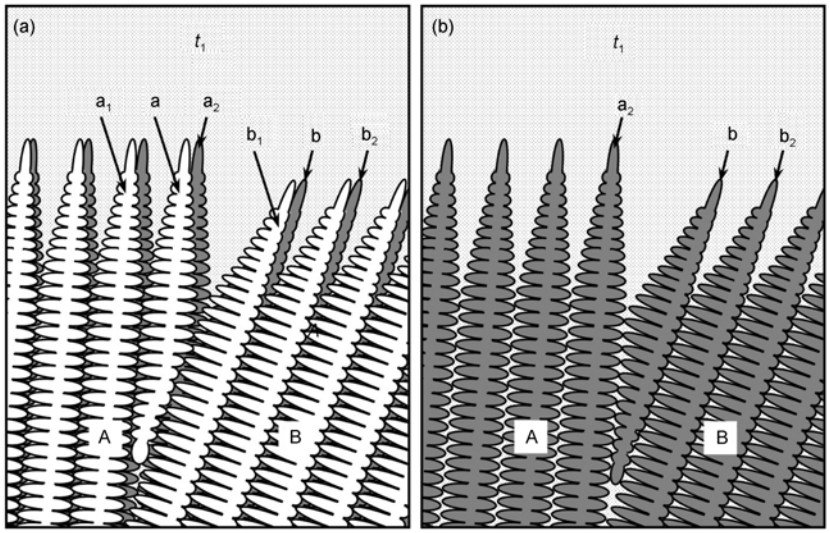

Figure 8 Schematic diagrams showing the branching effect in the open GB region of diverging grains. (a) Grain boundary structure containing two longitudinal planes at time t_1; (b) grain boundary structure containing one longitudinal plane at time t_1.

has no effect on branching and overgrowth mechanisms, and the GB misorientation (i.e. grain overgrowth rate) is thus independent of solidification rate.

This work was supported by the National Natural Science Foundation of China (Grant Nos. U1037601 and 50931004), the National Basic Research Program of China (Grant No. 2010CB631206) and the Program of "One Hundred Talented People" of the Chinese Academy of Sciences.

1 Walton D, Chalmers B. The origin of the preferred orientation in the columnar zone of ingots. Trans Metall Soc AIME, 1959, 215: 447–457
2 Mclean M. Directionally Solidified Materials for High Temperature Service. London: Metals Society, 1983. 1–9
3 Boettinger W J, Coriell S R, Greer A L, et al. Solidification Microstructures: Recent development, future directions. Acta Mater, 2000, 48: 43–70
4 Gandin C A, Eshelman M, Trivedi R. Orientation dependence of primary dendrite spacing. Metall Mater Trans, 1996, 27A: 2727–2739
5 Ding G L, Tewari S N. Dendritic morphologies of directionally solidified single crystals along different crystallographic orientations. J Cryst Growth, 2002, 236: 420–428
6 Boden S, Eckert S, Willers B, et al. X-ray radioscopic visualization of the solutal convection during solidification of a Ga-30 wt pct in alloy. Metall Mater Trans, 2008, 39A: 613–623
7 Arnberg L, Mathiesen R H. The real-time, high-resolution X-ray video microscopy of solidification in aluminum alloys. J Miner Met Mater Soc, 2007, 59: 20–26
8 Feng Q, Nandy T K, Tin S, et al. Solidification of high refractory ruthenium containing superalloys. Acta Mater, 2003, 51: 269–284
9 Liu L, Huang T W, Qu M, et al. High thermal gradient directional solidification and its application in the processing of nickel-based superalloys. J Mater Proc Techn, 2010, 210: 159–165
10 Luo W Z, Shen J, Li Q L, et al. Effects of growth rate on microstructure of directionally solidified Ti-43Al-3Si alloy with a seed technique. Acta Metall Sin, 2006, 42: 1238–1242
11 Meng X B, Li J G, Jin T, et al. Evolution of grain selection in spiral selector during directional solidification of nickel-base superalloys. J Mater Sci Technol, 2011, 27: 118–126
12 Zhou Y Z, Jin T, Sun X F. Structure evolution in directionally solidified bicrystals of nickel base superalloys. Acta Metall Sin, 2010, 46: 1327–1334
13 Yu J, Xu Q Y, Liu B C, et al. Experimental study and numerical simulation of directionally solidified turbine blade casting. J Mater Sci Technol, 2008, 24: 369–373
14 Pan D, Xu Q Y, Liu B C, et al. Modeling of grain selection during directional solidification of single crystal superalloy turbine blade castings. J Miner Met Mater Soc, 62: 30–34
15 Quested P N, Mclean M. Solidification morphologies in directionally solidified superalloys. Mater Sci Eng, 1984, 65: 171–180
16 Carter P, Cox D C, Gandin C A, et al. Process modelling of grain selection during the solidification of single crystal superalloy castings. Mater Sci Eng, 2000, 280A: 233–246
17 D'Souza N, Ardakani M G, McLean M, et al. Directional and single crystal solidification of Ni-base superalloys: Part I. The role of curved isotherms on grain selection. Metall Mater Trans, 2000, 31A: 2877– 2886
18 McLean M, Lee P D, Shollock B A. Origins of solidification defects during processing of nickel-base superalloys. In: Fuchs G, James A, Gabb T, et al., eds. Advance Materials and Processes for Gas Turbines, TMS, 2003. 83–90
19 Rappaz M, Gandin C A, Desbiolles J L, et al. Prediction of grain structures in various solidification processes. Metall Mater Trans, 1996, 27A: 695–705
20 Rappaz M, Gandin C A. A coupled finite-element cellular-automation model for the prediction of dendritic grain structures in solidification processes. Acta Metall Mater, 1994, 42: 2233–2246
21 Zhou Y Z, Volek A, Green N R. Mechanism of competitive grain growth in directional solidification of a nickel-base superalloy. Acta Mater, 2008, 56: 2631–2637
22 Zhang J, Singer R F. Effect of grain-boundary characteristics on castability of nickel-base superalloys. Metall Mater Trans, 2004, 35A: 939–946
23 Kurz W, Fisher D J. Fundamentals of Solidification. Aedermannsdorf, Switzerland: Trans Tech. Publishers, 1984. 51–88
24 Zhou Y Z, Green N R. Competitive grain growth in directional solidification of a nickel-base superalloy. In: Reed R C, Green K A, Caron P, et al., eds. Superalloys 2008. Warrendale, PA: TMS, 2008. 317–324